XiA: Send-it-Anyway Q-Routing for 6G-Enabled UAV-LEO Communications

Pallav Kumar Deb, *Graduate Student Member, IEEE*, Anandarup Mukherjee, *Graduate Student Member, IEEE*, and Sudip Misra, *Senior Member, IEEE*

Abstract—In this paper, we propose a delay-aware Q-learning-based routing algorithm - XiA - for sending data from users to nearest Access Points (APs) through Unmanned Aerial Vehicle (UAV) swarms communicating using 6G technology. These UAVs assist the ground networks in overcoming communication voids while maneuvering through different demographics. However, the communication links in the THz band have limited transmission range, causing the UAVs to frequently disconnect from the swarm. We overcome such issues by waiting until the UAV comes in contact with others in case of non-time-sensitive data. In the case of time-sensitive data, the UAVs send the data to the APs through Low Earth Orbit (LEO) satellites. To empower XiA to adapt to the changing environments and expensive delays in LEO, we model the rewards by accounting for spreading and absorption in the 6G channels, and Doppler effect and pointing error in the satellite channel. We show our bias for the parameters through extensive simulations and prove that the Q-model in XiA achieves convergence under all conditions. Additionally, in comparison with state-of-the-art solutions, we observe that XiA offers an improved delay of 82%.

Index Terms—Unmanned Aerial Vehicle swarms, Communication channel, Data offloading, Routing, Reinforcement learning, Q-learning, THz communication, Satellite communication, Mobility.

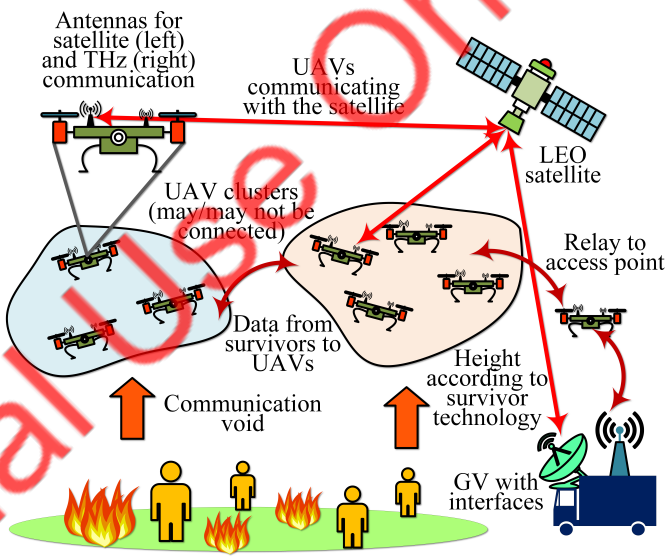

Figure 1: Proposed UAV-LEO-GV architecture for XiA.

1 Introduction

UAVs acting as aerial Base Stations (BSs) play a significant role in establishing network connection in *disaster-hit areas* and also in *overcoming communication voids*. Precise placement of Ground Vehicles (GV) on uneven terrains and hazardous regions for establishing communications is challenging. In such scenarios, it is beneficial for these GVs to deploy UAVs and receive data from them. The *limited channel capacities* among the UAVs often get *overloaded*, mandating the need for communications with higher capacities, implying the application of the THz band in 6G technologies. Although the increased frequency range offers improved data rates, the corresponding short wavelengths *limit the transmission range*. Such limitations restrict the movement of the UAVs to *ensure connectivity* with neighboring UAVs and nearest Access Points (APs)/GV. Additionally, the reduced communication ranges create disjoint sets of UAVs with no network path to the GV. While Low Earth Orbit (LEO) satellites (SAT) is a straightforward solution for overcoming the aforementioned issues, it is *expensive* (time consuming). Intelligent routines are necessary to determine the *data offloading* strategy for *minimizing* transmission delays in such mobile *real-time* environments.

In this work, we propose a Q-learning (QL)-based delay-aware solution - XiA - to route the data through the neighboring UAVs (multi-hops) to the nearest AP. XiA stands for *Send-it-Anyway* with X representing the ground, UAV, and space connections from the UAV. We assume that the APs in this work have interfaces for both 6G and satellite communications. We consider a set of UAVs $\mathcal{U} = \{u_1, u_2, ..., u_m\}$, deployed from GVs in communication voids or disaster-hit areas, form clusters based on their locations and transmission range as shown in Fig. 1. They communicate among one another and the GV using THz communications and receive data from a set of users/survivors $\mathcal{V} = \{v_1, v_2, ..., v_n\}$. Since the user devices may be of any type (4G/5G/6G), we do not restrict the user-UAV communication to one technology. However, the height of the UAVs depends on the type of communication link. These UAVs receive data from the users and forward/route it to the nearest GV/AP among the set $\mathcal{A} = \{a_1, a_2, ..., a_p\}$ via other neighboring UAVs

P. K. Deb, A. Mukherjee, and S. Misra are with the Department of Computer Science and Engineering, Indian Institute of Technology Kharagpur, India. e-mail: (pallv.deb,sudipm)@iitkgp.ac.in, anandarupmukherjee@ieee.org

acting as relays. UAVs that are away from its neighbors and lose connection with the APs may offload their data to the satellites. Since the delay for UAV-satellite communication is high, we offload to the satellite based on the time-sensitivity of user data. Such network architectures have the potential to enhance network connectivity, increase reliability and coverage of UAV services, perform Simultaneous Localisation and Mapping (SLAM) operations, and others. It may be noted that, as shown in Fig. 1, we consider UAVs and GVs to have both 6G and satellite communication technologies.

Example Scenario: We illustrate the proposed routing solution with the help of an example. Consider a disaster-hit region with users stranded on dangerous terrains such as in Fig. 1. Survivor tracking and management, along with GV placement, is challenging in such scenarios. UAVs deployed in these regions from the GV may identify survivors with onboard cameras, infrared and thermal sensors, and others. The proposed routing algorithm XiA, for the 6G-enabled UAVs using the QL method, facilitates optimized forwarding of the tracked information to the nearest GV. In case there is no connection to the GV, the UAVs offload the data to the satellite based on the data urgency. Otherwise, the UAV stores the information in its cache until the arrival of other proximal UAVs. We consider one AP/GV to establish a proof-of-concept for XiA. The same will work in case of the presence of multiple APs on the ground.

1.1 Motivation

UAVs operate in the 3D space with 6 degrees of freedom, implying that the environmental conditions have daunting effects on the flight parameters, which directly hamper the communication links due to the sensitivity of the THz bands. Such effects increase the difficulty of steady and planned flight, especially in disaster-hit areas and communication voids. In such conditions, reliable communication is necessary. Moreover, independently flying UAVs often get disconnected from the swarm, losing their communication path to the APs. In such scenarios, communication with LEO satellites is beneficial. However, high UAV-satellite communication costs (due to limited UAV resources) and increased delay mandate the need for intelligent routing decisions in real-time. Additionally, the limited transmission range in 6G technologies further increases the changes in the communication links in the swarm. These issues motivate us to design the proposed solution XiA, for intelligently routing time-sensitive data to nearest APs by accounting for the resource-constrained nature of the UAVs and the limitations in 6G, coupled with the delays in the LEO communications. Additionally, salient features of QL, such as the feedback loop, easy adaptation to changes, and the non-greedy selection technique motivate us to adopt it as the solution approach for this work.

1.2 Contribution

In this work, we propose a QL-based solution XiA, for routing delay-sensitive data packets from the users to the nearest APs using UAV BSs. The UAVs communicate using THz frequency band and communicate with LEO satellites to overcome limited transmission ranges and receive messages from the disjoint ones. The following constitute our major contributions in this work:

- ***UAV-LEO-GV Architecture:*** We present an architecture for maintaining communication with UAVs and the disjoint participants of the swarms that move out of the transmission range by enabling communication with LEO satellites. We also highlight possible network topologies for the proposed architecture.
- ***Delay-Sensitive Routing:*** We formulate reward functions based on the urgency of the data from the users and the communication links among the participants of the UAV swarms. We account for the dynamically changing environments and make informed decisions from past mistakes using Q-learning approach.
- ***Evaluation:*** Through extensive real-world emulations and by accounting for the atmospheric effects on the communication signals and changing topologies, we provide a detailed analysis of XiA.

It may be noted that we refrain ourselves from modeling the user-UAV interactions to maintain simplicity in this paper and focus on the UAV-UAV and UAV-LEO communications.

2 Related Work

The THz band's frequencies do not behave in the same way as the current GHz band due to small radio frequency (RF) components [1]. As the signals in such high frequencies demonstrate distinguishable spatio-temporal dispersion due to scattering, Ju *et al.* [2] designed channel models for THz communications. They studied the scattering power from various materials with different roughness factors. In addition to scattering, line-of-sight signals, reflection, and diffraction components also affect the received signal power. Han *et al.* [3] designed channel models for the THz band by considering the mentioned factors using ray-tracing techniques. Moreover, THz frequencies do not perform well on hardware impairments. The authors in [4] designed a channel estimator and signal detector to facilitate reliable data exchange. Apart from the channel models and applications mentioned above, the authors in [5] highlighted further opportunities and challenges in the THz band.

The frequencies in the THz band suffers from attenuation due to scattering and dispersion in the near-earth atmosphere [6]. Such attenuation effects mandate UAVs to fly close to the ground and also in close proximity to communicate with one another. The authors in [7] proposed methods for determining optimal atmospheric heights for seamless connectivity. They accounted for various environmental conditions such as temperature, water vapour, changing weathers, and others in their study. Gong *et al.* [8] proposed a scheme based on gradient projection to maximize network availability for free space optical satellites. Similarly, Yuichi *et al.* [9] proposed a resource allocation scheme for satellites serving requests from terrestrial, airborne, and marine devices/users. Apart from channel maximization, the authors in [10] addressed the issue of impairments in satellite hardwares. They focused on multi-beam antennas in the satellites along with propagation loss, and random

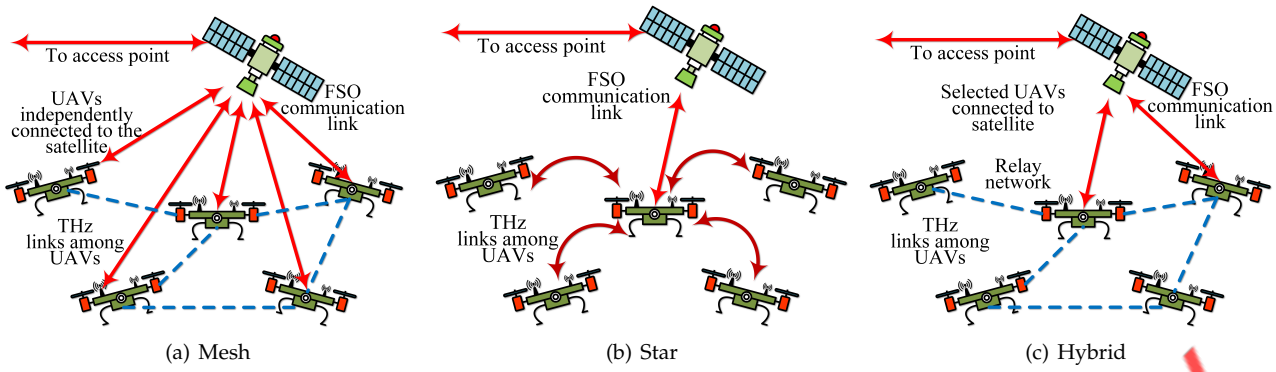

(a) Mesh (b) Star (c) Hybrid

Figure 2: Network topologies for the proposed routing scheme.

shadowing and investigated relay-based land-satellite communications. Jian *et al.* [11] also proposed a big data solution to identify behaviors of mobile BSs based on network data. The authors in [12] presented different gateway-selection methods for small and mini UAVs. Other applications of ML and its scope in wireless networks is featured in [13].

Synthesis: Routing in UAV swarms is a mature field of study among researchers. However, there exists a lacuna in these routing mechanisms for adapting to highly dynamic environments. Since communication links in conventional 4G and 5G technologies last for long ranges, the existing literature does not suffice for 6G communications. Intelligent solutions are necessary for the highly dynamic links among the UAVs and their network constraints due to the THz band. Conventional ground vehicle-UAV communications do not suffice for UAVs with real-time tasks that need to cover a large area. The limited communication range forces the UAVs to form disjoint components, which makes routing more challenging. In such cases, smart satellite communication is essential to route important messages to the nearest AP.

3 Network Architecture

We consider a set of UAVs $\mathcal{U} = \{u_1, u_2, ..., u_m\}$ and a set of user devices $\mathcal{V} = \{v_1, v_2, ... v_n\}$ in the network. We also consider a LEO satellite $\mathcal{L}$ to facilitate the communication with isolated UAVs. The formation of the UAVs from the GV, acting as flying BS, may be based on any of the three modes in Fig. 2. Due to the communications with the LEO satellites, the UAVs may not mandatorily be in connection with the nearest AP and neighboring UAVs. This relaxation in connectivity (dotted lines in Fig. 2(a)) allows extended coverage to the UAVs. In Fig. 2(b), the UAVs follow a star topology, where the master UAV is responsible for collecting data from the other UAVs and interacting with the LEO satellite. On the other hand, the UAVs in Fig. 2(a) follow a mesh topology, and all of them have the provision for connecting to the satellite. In such cases, each UAV is capable of making transmission decisions based on requirements. Fig. 2(c) is a hybrid deployment method where few selected UAVs may communicate with the satellite, and the other UAVs orchestrate the communication for delivering data to the APs through them. In this work, we consider the topology in Fig. 2(a) and the UAVs to be in connection with one another using THz communication technologies and free-state optical communication for the satellite. Communication with the user devices may be either THz or GHz communications. The decision on user device frequency range is important for determining the flight height and mobility of the UAVs.

4 System Model

4.1 UAV-UAV Communications

The THz band does not show the same characteristics as the GHz band in the conventional 4G and 5G networks. Although 6G technology offers increased channel capacities, the low wavelength restricts the communication range. This limitation increases the challenge of maintaining uninterrupted interaction between the UAVs. To model the channels connecting the UAVs, we consider both Line-of-Sight (LOS) and Non-Line-of-Sight (NLOS) signals. In case of LOS communication, the signals suffer due to spreading (A_{spr}) and molecular absorption (A_{abs}). Both (A_{spr}) and (A_{abs}) are functions of carrier frequencies (f_{6G}^{uav}) and distance (d_{6G}^{uav}). The expression for (A_{spr}) is:

$$A_{spr}(f_{6G}^{uav}, d_{6G}^{uav}) = \left(\frac{c}{4\pi f_{6G}^{uav} d_{6G}^{uav}}\right)^2 \quad (1)$$

where c is the speed of light in vacuum. On the other hand, the expression for (A_{abs}) is:

$$A_{abs}(f_{6G}^{uav}, d_{6G}^{uav}) = e^{-k(f_{6G}^{uav})d_{6G}^{uav}} \quad (2)$$

where $k(f_{6G}^{uav})$ is the molecular absorption coefficient at f_{6G}^{uav}. Combining equations 1 and 2, we calculate the path gain of the LOS signals (α_{LOS}) as:

$$\alpha_{LOS}^2 = \left(\frac{c}{4\pi f_{6G}^{uav} d_{6G}^{uav}}\right)^2 e^{-k(f_{6G}^{uav})d_{6G}^{uav}} \quad (3)$$

In case of NLOS signals, in addition to A_{spr} and A_{abs}, the signals depend on the reflection coefficient $(\mathcal{R}(f_{6G}^{uav}))$ which further depends on Fresnal reflection coefficient $(\mathcal{F}(f_{6G}^{uav}))$ and Rayleigh roughness factor $(\rho(f_{6G}^{uav}))$ accord-

ing to the expression: $\mathcal{R}(f_{6G}^{uav}) = \mathcal{F}(f_{6G}^{uav}).\rho(f_{6G}^{uav})$. We calculate $\mathcal{F}(f_{6G}^{uav})$ for smooth surfaces as:

$$\mathcal{F}(f_{6G}^{uav}) = \frac{cos(\theta_i) - n_{ri}\sqrt{1 - \left(\frac{1}{n_{ri}} sin(\theta_i)\right)^2}}{cos(\theta_i) + n_{ri}\sqrt{1 - \left(\frac{1}{n_{ri}} sin(\theta_i)\right)^2}} \quad (4)$$

where n_{ri} is the refractive index of the material and θ_i is the angle of incidence. We calculate $\rho(f_{6G}^{uav})$ as:

$$\rho(f_{6G}^{uav}) = exp\left(- \frac{8\pi^2 (f_{6G}^{uav})^2 \sigma^2 cos^2(\theta_i)}{c^2} \right) \quad (5)$$

where σ is standard deviation and follows Gaussian distribution [3]. Using equations 4 and 5, we calculate the NLOS path gain of the signals (α_{NLOS}) as:

$$\alpha_{NLOS}^2 = \mathcal{R}(f_{6G}^{uav}).A_{spr}(f_{6G}^{uav}, d_{6G}^{uav}).A_{abs}(f_{6G}^{uav}, d_{6G}^{uav}) \quad (6)$$

Adding equations 3 and 6, we calculate the effective channel gain $h(f_{6G}^{uav}, d_{6G}^{uav}))$ as:

$$h(f_{6G}^{uav}, d_{6G}^{uav})) = \alpha_{LOS} + \sum_{j=1}^{K_{NLOS}} \alpha_{NLOS,j} \quad (7)$$

The channel gain in equation 7 is an important factor in determining the data rate in the channel using the expression:

$$R_{dr}^{6G} = B_{6G} \times log\left(1 + \frac{p}{N_{JN}} (h(f_{6G}^{uav}, d_{6G}^{uav}))^2\right) \quad (8)$$

where B_{6G} is the bandwidth of the channel, p is power of the signal, and N_{JN} is the Johnson-Nyquist noise, such that $N = k_B \times T \times B_{6G}$. k_B is the Boltzmann constant and T is temperature. We use N_{JN} to represent the noise as the conventional Additive White Gaussian Noise does not effect THz band as it does in the GHz band.

Delay among the UAVs: In either use of communication technology (4G/5G/6G) by the user devices to connect to the UAVs, the data needs to travel to the UAV and then reach the destination access point through multi-hops through the UAVs or via the satellite link. As mentioned earlier in Section 1.2, we focus only on the data transmission among the UAVs. For data transmission from UAV i to j, we account for the time for transmitting the data $(t_{trans}^{UAV_j})$, waiting time at the queue of the receiving UAV $(t_{wait}^{UAV_j})$, and the time for processing $(t_{head}^{UAV_j})$ the packet headers to determine forwarding rules. Using equation 8, for data of size $S_d^{UAV_i}$ from a UAV, $t_{trans}^{UAV_j} = \frac{S_d^{UAV_i}}{R_{dr}^{6G}}$. The queueing delay of each data from i^{th} UAV is dependent on the arrival $(\mathbb{A}_j)$ and forwarding rate $(\mathbb{F}_j)$ at the receiving j^{th} UAV. From statistical analysis in [14], we consider $\mathbb{A}_j$ to follow a Poisson distribution and calculate the waiting time as $t_{wait}^{UAV_j} = 1/(\mathbb{F}_j - \mathbb{A}_j)$ [15]. The header reading time is dependent on the clock cycles $(p_{freq}^{UAV_j})$ of the UAV processor and is calculated as $t_{head}^{UAV} = \frac{S_d^{pkt_i}}{p_{freq}^{UAV_j}}$. In summary, the transmission time of the data from UAV i to j is: Time needed for transmission:

$$t_{6G}^{UAV_{ij}} = x_{ij}(t_{trans}^{UAV_j} + t_{wait}^{UAV_j} + t_{head}^{UAV_j}) \quad (9)$$

where x_{ij} is a binary variable that takes the value 1 for transmitting from UAV i to j and 0 otherwise.

4.2 UAV to LEO satellite

The signals travelling from an UAV to a satellite suffers from three phenomenons: 1) Doppler effect (Δf_{LEO}^{UAV}), 2) Pointing error (f_{LEO}^{PE}), and 3) Atmospheric turbulence (f_{LEO}^{AT}). The UAVs fly at a certain height (h_{UAV}) from the Earth's surface, due to which the radius logically increases. We calculate the radius as $R_{UAV} = (r_e + h_{UAV})$. From R_{UAV}, the shift in frequency due to the the Doppler effect is:

$$\Delta f_{LEO}^{UAV} = \frac{f_{LEO}^{UAV} d_{LEO} R_{UAV} v_a sin(v_a t)}{c\sqrt{d_{LEO}^2 + R_{UAV}^2 - 2 d_{LEO} R_{UAV} cos(v_a t)}} \quad (10)$$

where f_{LEO}^{UAV} is channel frequency of UAV to the LEO satellite, d_{LEO} is distance of the satellite from center of earth, v_a is angular velocity of UAV, and t is time of flight with v_a. Pointing error is typically negligible for terrestrial base stations that are stationary. On the contrary, UAVs fly freely with 6 degrees of freedom. This makes pointing error an important factor for UAVs as they are not steady, giving rise to scintillation. We calculate the pointing error as:

$$f_{LEO}^{PE}(r_b) = \frac{r_b}{\phi^2} exp\left(- \frac{r_b^2 + \psi^2}{2\phi^2} \right) I_0\left(\frac{r_b \psi}{\phi^2} \right) \quad (11)$$

where r_b is the beam radius, for angular deviations ϕ_j and ψ_j are calculated as $\phi = \phi_j d_{lnk}$ and $\psi = \psi_j d_{lnk}$ with d_{lnk} as the length of the link. The d_{lnk} is mathematically represented as $d_{lnk} = (d_{LEO} - h_{UAV}) sec(z)$ where z is the zenith angle. The distribution of atmospheric turbulence may be a gamma-gamma distribution or log-normal distribution [16]. As the log-normal distribution is popularly accepted for atmospheric turbulence, we calculate it as:

$$f_{LEO}^{AT}(\mathcal{C}) = \frac{1}{\mathcal{C}\varrho_1\sqrt{2\pi}} exp\left(- \frac{[ln(\mathcal{C}) + 0.5\varrho_1^2]^2}{2\varrho_1^2} \right) \quad (12)$$

where $\varrho_1 = exp(\omega_1 + \omega_2) - 1$ and

$$\omega_1 = \frac{0.49\varrho_2^2}{(1 + 0.18d^2 + 0.56\varrho_2^{12/5})^{7/6}}$$

$$\omega_2 = \frac{0.51\varrho_2^2 (1 + 0.69\varrho_2^{12/5})^{-5/6}}{1 + 0.9d^2 + 0.62d^2\varrho_2^{12/5}}$$

where $d = \sqrt{kD^2/4d_{lnk}}$ with $k = 2\pi/\lambda$ and $\varrho_2^2 = 0.492k^{7/6} S_{ATM}^2 L^{11/6}$. Here, λ is the wavelength and S_{ATM} is the strength of the atmospheric turbulence, respectively. Using equations 10, 11, and 12, we calculate the effective satellite channel gain (h_S) as:

$$h_S = \Delta f_{LEO}^{UAV} . f_{LEO}^{PE}(r_b) . f_{LEO}^{AT}(\mathcal{C}) \quad (13)$$

Similar to the argument in Section 4.1, we calculate the Data rate in the UAV to satellite channels as:

$$R_{dr}^{LEO} = B_{LEO} \times log\left(1 + \frac{p_{LEO}}{N_{AWGN}} (h_S(f_{LEO}^{uav}, d_{LEO}^{uav}))^2\right) \quad (14)$$

where B_{LEO} is the bandwidth, p_{LEO} is power of the signal, and N_{AWGN} is the additive white Gaussian noise.

Delay for UAV-LEO-GV Communications: We account for the uplink transmission of data from the UAVs to the satellites

(t_{up}^{LEO}), the downlink transmission from the satellites to the nearest AP (t_{down}^{LEO}), and the queueing delay at the satellite (t_{wait}^{LEO}). We calculate the uplink delay for transmitting data of size S_d^{UAV} to the satellites as $t_{up}^{LEO} = \frac{S_d^{UAV}}{R_{dr}^{LEO}}$. The expression for t_{down}^{LEO} remains the same as that for t_{up}^{LEO} with corresponding R_{dr}^{LEO}. We calculate t_{wait}^{LEO} using the same arguments as in Section 4.1 as $t_{wait}^{LEO} = 1/(\mathbb{F}_{LEO} - \mathbb{A}_{LEO})$, where $\mathbb{F}_{LEO}$ and $\mathbb{A}_{LEO}$ are the forwarding and arrival rates at the satellite. Using these expressions, we calculate the delay for the UAV-LEO-AP communication as:

$$t_{AP}^{LEO} = t_{up}^{LEO} + t_{wait}^{LEO} + t_{down}^{LEO} \tag{15}$$

The power of the downlink signal from the satellites is relatively more powerful than that of the uplink signal [17].

4.3 Energy Consumption at the UAV

UAVs have to keep rotors running throughout their deployment, which needs significant amount of energy. Moreover, the UAVs in this work act as BS for user devices, which involves data reception and forwarding (to neighbor UAV or satellite). We propose reserving some energy (E_{ret}^{RES}) for the UAVs to return back to their base, which is dependent on its position at time t. We allow the drones to operate under the proposed scheme only when the residual energy of the i^{th} UAV at time t ($RE_i(t)$) along with $E_{ret}^{RES_i}(Pos_t)$ satisfies the following condition:

$$RE_i(t) - E_{ret}^{RES_i}(Pos_t) > t_{flight}^{i} e_{flight}^{i} + w t_{6G}^{UAV_{ij}} e_{6G}^{UAV_{ij}} + (1-w) t_{up_i}^{LEO} e_{up_i}^{LEO} \tag{16}$$

where w is a binary variable that determines whether to forward the data to neighboring UAV or to the satellite. We discuss the policy for determining the value of w in the subsequent sections. Variables t_{flight}, $t_{6G}^{UAV_{ij}}$, and $t_{up_i}^{LEO}$ represent the flight and forwarding (UAV/satellite) times. The e_{flight}^{i}, $e_{6G}^{UAV_{ij}}$, and $e_{up_i}^{LEO}$ are the corresponding energy decrement rates. It may be noted that we exclude the energy for reception of the signals. This is because power from the receiving signal opens scope for new research works that deal with energy harvesting and deflecting. Both the methods have the potential to save energy as well as reduce its consumption. Satellites on the other hand are equipped with solar panels, which supply abundant amount of energy to provide uninterrupted data transfer services and hence we assume its seamless availability.

4.4 Cost and Reward Functions

We first define the cost function pertaining to each UAV for forwarding the data to the next UAV or to the AP. We design the UAVs to be aware of the time sensitivity nature of the data from the users and from neighboring UAVs. The cost function ($\mathcal{C}_i^{UAV}$) for each UAV is dependent on the time for forwarding the data to the next UAV in equation 9 or to the satellite in equation 15. Mathematically,

$$\mathcal{C}_{u_i}^{UAV} = w t_{6G}^{UAV} + (1-w) t_{LEO}^{UAV} \tag{17}$$

We define the reward function based on the cost in equation 17. The system reward is only maximized when each UAV minimizes its data forwarding cost, implying $min\ \mathcal{C}_{u_i}^{UAV} \forall u_i \in \mathcal{U}$. We define the reward of Q-learning system for determining the data forwarding as:

$$max \sum_{i=1}^{m} R_{u_i} = \frac{e^{1-\mathcal{C}_{u_i}^{UAV}}}{1 - e^{1-\mathcal{C}_{u_i}^{UAV}}} \tag{18}$$

The reward/objective function in equation 18 satisfies the constraints in equation 16. Additionally, we also ensure that the UAVs have enough cache memory (M_{cache}^{res}) to receive the data from users or from other neighboring UAVs.

4.5 Methodology

We consider deployment of the UAVs to overcome communication voids in the network, implying the availability of minimal number of proximal APs on the ground. We train our Q-learning model to forward the data to the nearest AP through multi-hops across the UAVs in the network. However, based on tasks and location of the UAVs, they may not be in contact with other UAVs or in some cases, an entire cluster of UAVs may not be able to reach the ground APs. We design our weights (w) in equation 17 as a function of type of the time-sensitivity of the data from u_i (τ_{u_i}). In the case of non-time-sensitive data, we wait for the UAVs to come in contact with other UAVs ($w = 1$) which have connection with the APs. In case of urgency, we forward the data directly to the satellite ($w = 0$). Thus, In this work, we consider $\tau_{u_i} = 0.5$ for proof of concept. In summary,

$$w(\tau_{u_i}) = \begin{cases} 1, & \text{UAV-UAV communication.} \\ 0, & \text{UAV-LEO communication.} \end{cases} \tag{19}$$

XiA may identify loops during route planning when there is no path to the AP. In such situations, we directly assign $w = 0$. In the worst case, XiA needs $\mathcal{O}(\mathcal{U}^3)$ time for learning, where $\mathcal{U}$ is the number of UAVs. Further, we use a value iteration-based RL model. For S states and $\mathcal{A}$ actions, XiA has a computational complexity of $\mathcal{O}(\mathcal{A}.\mathcal{S}^2)$ as it depends quadratically on $\mathcal{S}$ and linearly on $\mathcal{A}$ [18].

5 Performance Evaluation

We derive the parameters pertaining to LEO communications based on the works of Di *et al.* [17] to maintain simplicity and to avoid repetition. We then present the results concerning the channel characteristics and the performance of the proposed algorithm (XiA) compared to existing state-of-the-art algorithms (Dijkstra).

5.1 Simulation Setup

In this work, we simulate the movement of the UAVs using popularly available mobility models. Typically, Random Waypoint and Gauss-Markov mobility models are the most popularly used mobility models for Mobile Ad-hoc Networks (MANETs). In this work, we are particularly interested in simulating the movement of the UAVs, which involves movement in 3D space. Moreover, since the UAVs may move smoothly as well as abruptly, we require a mobility model that offers the flexibility to do so. We consider the above mentioned constraints and opt for the Gauss Markov Mobility Model [19] to represent the movement of

Table 1: Simulation parameters.

Parameter	Value
Simulation area	$10 \times 10\ Km^2$
Communication range (6G)	3 m
Center frequency (6G)	$0.5 - 10$ THz
Bandwidth (6G)	$200 - 350$ GHz
Transmission power (6G)	10 dBm
Gamma	0.8
Data rate (LEO) [17]	4.9 Gbps
Receiver antenna	10×10 Planar array
Data Size	$250 - 500$ Mb

the deployed UAVs. This mobility model calculates the $< x, y, z >$ coordinates of the UAV according to the equation $Pos^{t+1}_{x,y,z} = \xi Pos^{t}_{x,y,z} + (1-\xi)\overline{Pos}_{x,y,z} + \sqrt{(1-\xi^2)}Pos^{t}_{x,y,z}$ where $Pos_{x,y,z}$ represents the $< x, y, z >$ coordinates each at time instant t and $\overline{Pos}_{x,y,z}$ is the mean coordinate position. The parameter ξ determines the variability in the motion. Each of the UAVs vary their speed (s), direction (θ), and pitch (p) as $Pf^{t+1}_{s,\theta,p} = \xi Pf^{t}_{s,\theta,p} + (1-\xi)\overline{Pf}_{s,\theta,p} + \sqrt{(1-\xi^2)}Pf^{t}_{s,\theta,p}$ where ξ has its usual meaning. We set the simulation parameters in Table 1 while executing XiA. As we present our observations, we explain our bias towards selection of the primary parameters.

5.2 Results

5.2.1 Effect Due to Molecular Absorption

We present the observations on the effect of molecular absorption on the signal using the values of A_{abs} in equation 2. We observe the effects fue to A_{abs} in Fig. 3 with varying center frequencies ($0.5 - 10$ THz) and distances ($1 - 10$ meters). We observe that A_{abs} gives rise to spectral windows in that have gains below -40 dB. We observe minor absorption effects in the signals on using 3, 4, and 10 THz and a little higher effect in the case of 9 THz. However, we observe a significant drop of below -120 dB in the signal in the case of 6 THz center frequency. We comment that as the center frequencies get higher, the A_{abs} gives rise to efficient frequency windows that have the potential of transmitting signals with minimal effects. Based on the transmission distance, one may have a clear idea on which frequency range to use. Interestingly, the trend remains the same across all frequency ranges as we increase the distance. However, as the distance increases, the effect of A_{abs} increases significantly, specially above 5 meters.

Implication: The selected communication radius of 3 meters suffers from a maximum of -30 dB gain in all center frequencies (from $1-10$ THz), which enables us in assigning any sub-channel in an OFDM [20] modulation setup.

5.2.2 Effect Due to Spreading

We present the observations on the effect of spreading on the signal using the values of A_{spr} in equation 1. Fig. 4 depicts the spreading effects with varying frequencies (up to 10 THz) over distances up to 10 meters. We observe that the signals are less effected over short distances. However, the signal quality drops rapidly as we increase the center frequency. For instance, for a distance of 1 meter, the spreading phenomenon effects the signal by almost 20%. It is beneficial to keep low transmission distances to minimize

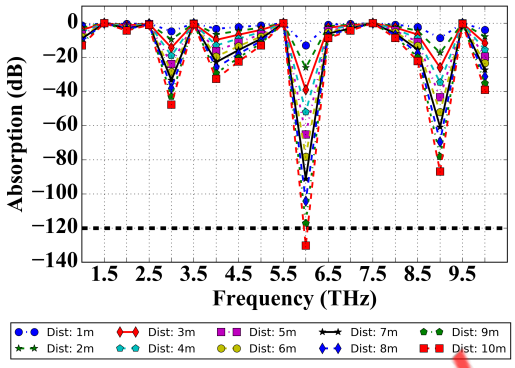

Figure 3: Effect of molecular absorption on the signal in the atmosphere with changing frequencies and distances.

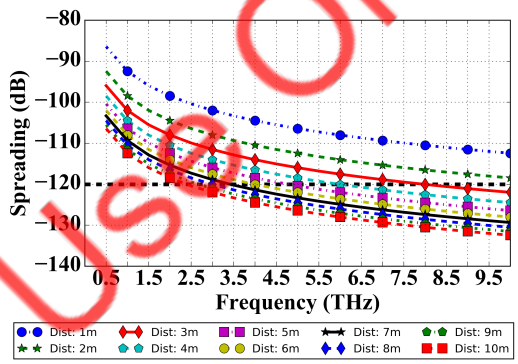

Figure 4: Effect of spreading on the signal with changing frequencies and distances.

effects due to A_{spr} and a center frequency below 5 THz. As we approach 10 meters, we observe an instantaneous drop to below -120 dB on going beyond 2 THz.

Implication: In this work, we consider a maximum transmission range of 3 meters, as discussed in Section 5.2.6. This value of the communication range helps in limiting the effects due to A_{spr} to below -120 dB for a wide range of center frequencies. Typically, we observe safe usage of up to 7 THz in Fig. 4. We may also go beyond to higher frequencies, which we present on studying the overall path gain in the next section.

5.2.3 Path Gain

We present the overall path gain based on equation 7 in Fig. 5 with varying frequencies and distances. Similar to that in Fig. 3, we observe spectral windows in Fig. 5. However, we notice that the quality of the signal drops below -40 dB on taking the overall effect of the environment on the signal into account. We comment in a similar fashion as in Section 5.2.1 that selection of center frequencies based on the transmission range in beneficial, particularly in the ranges $[0.5 - 2.5]$, $[3.5 - 5.5]$, $[6.5 - 8.5]$, and $[9.5 - 10]$ THz. For distances of up to 4 meters, we observe a path gain above -80 dB and those above 4 meters show signals dropping to less than -130 dB. Moreover, we observe similar trends for all the distances as in Fig. 3. Further, as we increase the

distance, the path gain decreases significantly. For instance, as we increase the distance of 3 meters to 10 meters, we observe an effect of more than 60%.

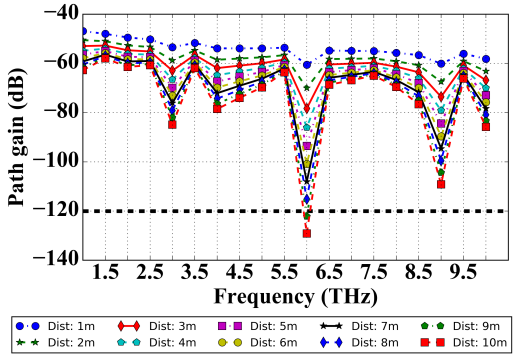

Figure 5: Overall path gain in the THz band.

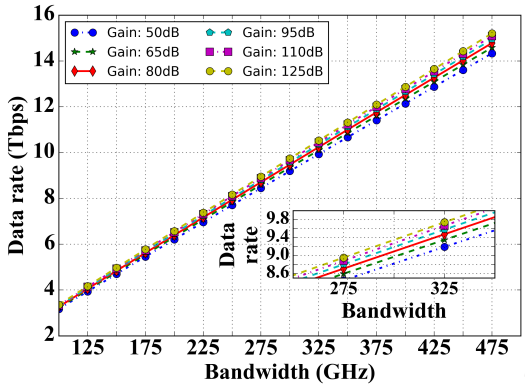

Figure 6: Data rate among the UAVs.

Implication: We observe in Fig. 5 that the transmission range of 3 meters offers a maximum drop of the signal to -80 dB at 6 THz center frequency. On the other hand, the path gain remains below -80 dB for all other frequencies. We safely fixate from our discussions in Sections 5.2.6 and 5.2.3 to a transmission range of 3 meters. This range allows efficient formation of network components among the UAVs in Fig. 8(c) as well as connectivity to the AP in addition to a maximum path gain of -80 dB.

5.2.4 Data Rate

Using the parameters for finding the path gain in equation 7, we find the data rate with varying bandwidths using equation 8. Fig. 6 depicts the possible data rates for the UAV-UAV communications. Since we use 6G communication technology, the bandwidth for each device is much higher than the conventional 4G and 5G technologies. We vary the bandwidth in the range of $100 - 500$ GHz and observe data rates as high as 15 Tbps. As we vary the gain in our channel, we observe a linearly increasing data rate. Based on these values, we run our simulation and calculate delays.

Implication: Although higher bandwidths yield better data rates, it also reduces the transmission range. Taking the tradeoff into account, we limit our bandwidth to $200 - 350$ GHz for our simulations and present the results.

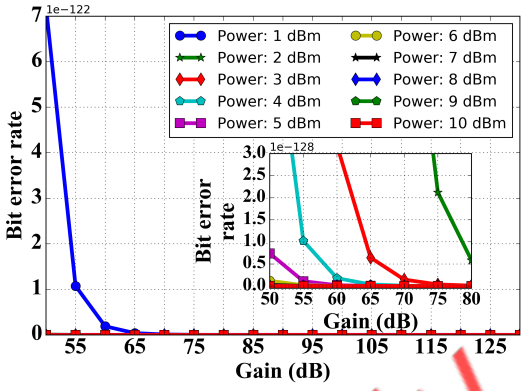

Figure 7: Bit error rate among the UAVs.

5.2.5 Bit Error Rate

We consider the UAVs to be equipped with omni-directional (N) planar antennas. For the UAVs in the air, they receive signals from the proximal UAVs along its cross section which may approximately contain N antennas. We calculate the bit error rate (BER) in the UAVs using $BER = \binom{2N-1}{N} \times (\frac{1}{2SNR})^2$, where SNR is the Signal to Noise Ratio and present the numerical results in Fig. 7. We observe that the BER in the THz band is minuscule. As we increase the channel gain, the BER further decreases. As we vary the power of the transmitted signal, the same trend remains the same for all values. As expected, we observe that the BER is minimal for 10 dBm signal power.

Implication: We set the power of the signals from the UAVs at 10 dBm as it has the minimal BER. Although such increased transmission power consumes a lot of battery power, it decreases the BER significantly as the data arrives at a very high rate. We plan to address optimized power allocation according to the distance of neighboring UAVs in the future.

5.2.6 UAV Connectivity

We take an instant of 50 UAVs operating in our simulation area and present them in Fig 8. It may be noted that although the UAVs in this work have 3D coordinates, Fig 8 depicts the top-view of our deployment area. We represent the UAVs as red circles/nodes and an AP at the center of the right corner edge in blue. The overlapping UAVs do not represent crashes as they are flying at different heights. We vary the communication range from $1 - 5$ meters in Figs. 8(a)–8(e). We observe that for 1 (Fig. 8(a)) and 2 (Fig. 8(b)) meters communication range, the UAVs form multiple disjoint components/clusters that do not have a path to the AP. Such communication ranges forces the UAVs to always opt for the satellite communication, which is expensive (in terms of delay) and rapidly drains the batteries. On the other hand, in the case of 4 (Fig. 8(d)) and 5 (Fig. 8(e)) meters communication range, we observe that the UAVs are over-connected with links, which causes interference in the signals. On the other hand, in the case of the 3 meter communication range, a majority of the UAVs have a path to the AP and give rise to only a small number of clusters. Moreover, although beyond the scope of this work, the clusters in the 3 meter communication range are

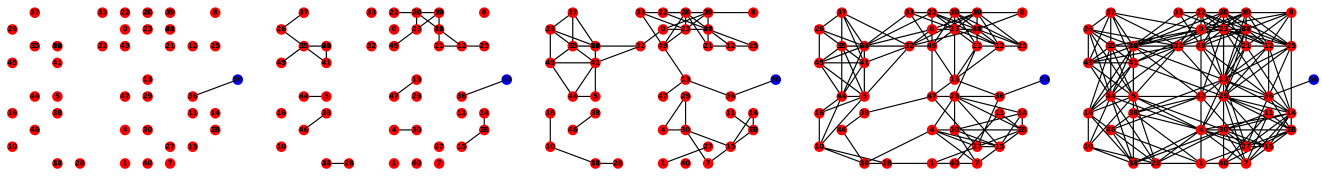

(a) Range: 1m (b) Range: 2m (c) Range: 3m (d) Range: 4m (e) Range: 5m

Figure 8: Comparison for connectivity among 50 UAVs (red) with varying communication ranges in 3D space with one access point (blue) as sink.

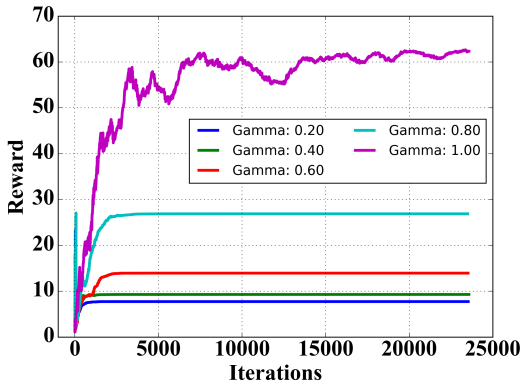

Figure 9: Rewards while training the model with changing gamma (exploration coefficient) values.

large enough to allow the formation of cluster heads to collect and transmit data from the proximal UAVs to the satellite. It may be noted that as we increase the number of UAVs in the network, the connectivity in the swarm will improve, resulting in lesser number of disconnected clusters and improved paths to the AP. Such conditions will help in reducing the delays for data forwarding.

Implication: We account for the effects of molecular absorption, spreading, and path gain of the signals in the THz band discussed in Sections 5.2.1, 5.2.2, and 5.2.3. We also consider the bit error rate (Section 5.2.5) and avoid the issues of multiple disconnected components and over connectivity by assigning a communication range of 3 meters (Fig. 8(c)) for the UAVs, which has a perfect balance for the connected and disjoint components. The UAVs that have a path to the AP through intermediate relays use the UAV-UAV communication to forward the data. In contrast, the UAVs in the disconnected components forward the data using UAV-LEO communications. It may be noted that although the 4 meter range has better connectivity (Fig. 8(d)), the additional 1 meter has significant effect on the quality of signal.

5.2.7 Rewards

We set the rewards in the R matrix of the Q-learning model according to equation 18. As the reinforcement learning model gives us the flexibility of deciding the intensity of dependency on immediate and future rewards using the $Gamma$ variable, we present our bias for its selection. Fig. 9 presents the rewards on training with different $Gamma$ values. We observe that we achieve convergence on all values of $Gamma$. However, in the case of $Gamma = 1$, the reward values are fluctuating and still shows an increasing trend on running for 25000 iterations.

Implication: Although we observe convergence for all $Gamma$ values, we select the one that achieves highest rewards while reaching convergence, implying $Gamma = 0.8$. The rest of the results are based on the observations from this $Gamma$ value.

5.2.8 Delay and Hop Count

We present our observations on executing XiA and comparing it with the state-of-the-art Dijkstra's shortest path algorithm and routing in Flying ad-hoc network using RL (FANRL) [21]. FAN-RL is a similar approach on a 5G environment and we consider bandwidths of 100-400 MHz with transmission ranges of 30 meters, transmission power of 10 dB, and unit noise for simulation. Interference and noise does not effect 6G communications in the same way as it does in conventional communication technologies in the GHz band. Accordingly, we relax the communication constraints and focus on the links and the shortest path available, for which, Dijkstra's algorithm is the most popular technique. Since the proposed work is tailored to be delay-aware, we focus on the transmission delays and the corresponding hop counts for both cases. We observe similar results for XiA and Dijkstra's algorithms when there exists only one path from the subject UAV and the AP. We also observe similar results when the UAVs offload their data to the satellite. In all the other cases, we observe that XiA offers better delays as XiA accounts for a number of features like the channel conditions and device configurations in addition to distance. On the other hand, Dijkstra's algorithm only depends on the distance between the UAVs. We tabulate our results pertaining to lower delays in case of XiA in Table 2. Although the number of hops is the same for both XiA and Dijkstra, we observe that XiA reduces the delay by a maximum of 15.51% and a minimum of 4%. Moreover, we observe in the fifth (second last) row that the Dijkstra's algorithm sometimes fails to find the shortest path and opts for sending the data to the satellite. This selection of the satellite increases the delay by 99% and also consumes a significant amount of battery, which although rarely occurs, it is undesirable. In the last row we observe that both XiA and Dijkstra's algorithm opt for the satellite, which renders equal delays. This is because no other path exists to the AP. On the other hand, in comparison with FAN-RL, we observe 99% improvement in delays in all cases. Although no satellite communications is necessary because of the longer communication links, the higher delays are because

Table 2: Comparison of XiA with existing state of the art solutions.

XiA Delay (s)	Dijkstra Delay (s)	FAN-RL Delay (s)	Improvement (Dijkstra)	Improvement (FAN-RL)	XiA Hops	Dijkstra Hops	FAN-RL Hops	XiA-LEO	Dijkstra-LEO	FAN-RL-LEO
1.78e-10	2.10e-10	1.42e-06	15.23%	99.98%	6	6	3	✗	✗	✗
1.94e-10	2.25e-10	8.88e-07	13.77%	99.97%	5	5	3	✗	✗	✗
1.37e-10	1.57e-10	1.09e-06	12.73%	99.98%	5	5	3	✗	✗	✗
3.63e-10	3.79e-10	1.42e-06	4.42%	99.97%	8	8	3	✗	✗	✗
1.96e-10	2.04e-07	7.94e-07	99%	99.97%	5	–	2	✗	✓	✗
1.62e-07	1.62e-07	9.5e-07	0%	82.94%	–	–	3	✓	✓	✗

of the lower bandwidths (in the MHz range). In the last row, even though XiA could not find a direct route to the AP, it demonstrates an 82% improvement over FAN-RL. We also notice lower number of hops (2-3) in FAN-RL due to longer communication ranges. It may be noted that we run our experiments multiple times and discuss on the minimum delays and situations when there are no paths to the AP.

Implication: We conclude that XiA outperforms conventional shortest path algorithms in terms of delays by notable margins, which is the main motive of this work. We also comment that XiA has the potential to find the fastest path in the presence of multiple other paths. The improvement over FAN-RL is well expected and is the main reason for adopting 6G networks and features such as beamforming, small cells, and MIMO are best fit for UAV networks.

6 Conclusion

In this work, we proposed a QL-based routing algorithm named Send-it-Anyway (XiA). The X in XiA represents any mode of communication. We considered a communication void or disaster-hit area where the UAVs deployed from a GV send data to a nearest AP. Towards this, we designed a reward function that minimises the time required for forwarding the data to the AP through multiple relay UAVs by considering the channel conditions and device configurations. In case the UAVs do not have a path to the AP, they send the data to a LEO satellite which then forwards the data to the AP. Through extensive simulations, we presented our bias for the simulation parameters and demonstrated how XiA performs in comparison to the state-of-the-art Dijkstra's algorithm. In comparison with state-of-the-art solutions, we demonstrated that XiA offers an improved delay of 82%. In the future, we plan to extend this work by incorporating more ground-level APs. We also plan to use group mobility models to observe the behavior of XiA under different conditions.

References

[1] F. Sheikh, Y. Gao, and T. Kaiser, "A Study of Diffuse Scattering in Massive MIMO Channels at Terahertz Frequencies," *IEEE Transactions on Antennas and Propagation*, vol. 68, no. 2, pp. 997–1008, Feb. 2020.

[2] S. Ju, S. H. A. Shah, M. A. Javed, J. Li, G. Palteru, J. Robin, Y. Xing, O. Kanhere, and T. S. Rappaport, "Scattering Mechanisms and Modeling for Terahertz Wireless Communications," in *Proceedings of IEEE International Conference on Communications (ICC)*, May 2019, pp. 1–7.

[3] C. Han, A. O. Bicen, and I. F. Akyildiz, "Multi-Ray Channel Modeling and Wideband Characterization for Wireless Communications in the Terahertz Band," *IEEE Transactions on Wireless Communications*, vol. 14, no. 5, pp. 2402–2412, May 2015.

[4] T. Mao, Q. Wang, and Z. Wang, "Spatial Modulation for Terahertz Communication Systems With Hardware Impairments," *IEEE Transactions on Vehicular Technology*, vol. 69, no. 4, pp. 4553–4557, Feb. 2020.

[5] T. S. Rappaport, Y. Xing, O. Kanhere, S. Ju, A. Madanayake, S. Mandal, A. Alkhateeb, and G. C. Trichopoulos, "Wireless Communications and Applications Above 100 GHz: Opportunities and Challenges for 6G and Beyond," *IEEE Access*, vol. 7, pp. 78 729–78 757, Jun. 2019.

[6] Q. Jing, D. Liu, and J. Tong, "Study on the Scattering Effect of Terahertz Waves in Near-Surface Atmosphere," *IEEE Access*, vol. 6, pp. 49 007–49 018, Aug. 2018.

[7] H. Li, Z. Wu, Z. Zhao, L. Lin, C. Lu, and T. Qu, "Modified model of equivalent height for predicting atmospheric attenuation at frequencies below 350 GHz," *IET Microwaves, Antennas Propagation*, vol. 12, no. 8, pp. 1420–1427, Jun. 2018.

[8] S. Gong, H. Shen, K. Zhao, R. Wang, X. Zhang, T. De Cola, and J. A. Fraier, "Network Availability Maximization for Free-Space Optical Satellite Communications," *IEEE Wireless Communications Letters*, vol. 9, no. 3, pp. 411–415, Mar. 2020.

[9] Y. Kawamoto, T. Kamei, M. Takahashi, N. Kato, A. Miura, and M. Toyoshima, "Flexible Resource Allocation With Inter-Beam Interference in Satellite Communication Systems With a Digital Channelizer," *IEEE Transactions on Wireless Communications*, vol. 19, no. 5, pp. 2934–2945, Jan. 2020.

[10] K. Guo, M. Lin, B. Zhang, W. Zhu, J. Wang, and T. A. Tsiftsis, "On the Performance of LMS Communication With Hardware Impairments and Interference," *IEEE Transactions on Communications*, vol. 67, no. 2, pp. 1490–1505, Feb. 2019.

[11] D. Jiang, L. Huo, and H. Song, "Rethinking Behaviors and Activities of Base Stations in Mobile Cellular Networks Based on Big Data Analysis," *IEEE Transactions on Network Science and Engineering*, vol. 7, no. 1, pp. 80–90, Jan. 2020.

[12] J. Wang, C. Jiang, Z. Han, Y. Ren, R. G. Maunder, and L. Hanzo, "Taking Drones to the Next Level: Cooperative Distributed Unmanned-Aerial-Vehicular Networks for Small and Mini Drones," *IEEE Vehicular Technology Magazine*, vol. 12, no. 3, pp. 73–82, Jul. 2017.

[13] J. Wang, C. Jiang, H. Zhang, Y. Ren, K. C. Chen, and L. Hanzo, "Thirty Years of Machine Learning: The Road to Pareto-Optimal Wireless Networks," *IEEE Communications Surveys & Tutorials*, vol. 22, no. 3, pp. 1472–1514, Jan. 2020.

[14] A. Mukherjee, S. Misra, A. Sukrutha, and N. S. Raghuwanshi, "Distributed Aerial Processing for IoT-Based Edge UAV Swarms in Smart Farming," *Computer Networks*, vol. 167, p. 107038, Nov. 2019.

[15] D. Gross, J. F. Shortle, J. M. Thompson, and C. M. Harris, *Fundamentals of Queueing Theory*, 4th ed. USA: Wiley-Interscience, 2008.

[16] H. D. Trung, D. T. Tuan, and A. T. Pham, "Pointing error effects on performance of free-space optical communication systems using SC-QAM signals over atmospheric turbulence channels," *AEU - International Journal of Electronics and Communications*, vol. 68, no. 9, pp. 869 – 876, 2014.

[17] B. Di, H. Zhang, L. Song, Y. Li, and G. Y. Li, "Ultra-Dense LEO: Integrating Terrestrial-Satellite Networks Into 5G and Beyond for Data Offloading," *IEEE Transactions on Wireless Communications*, vol. 18, no. 1, pp. 47–62, Dec. 2019.

[18] L. P. Kaelbling, M. L. Littman, and A. W. Moore, "Reinforcement Learning: A Survey," *Journal of artificial intelligence research*, vol. 4, pp. 237–285, May 1996.

[19] J. P. Rohrer, E. K. Çetinkaya, H. Narra, D. Broyles, K. Peters, and J. P. G. Sterbenz, "AeroRP performance in highly-dynamic airborne networks using 3D Gauss-Markov mobility model," in *Proceedings of Military Communications Conference (MILCOM)*, Nov. 2011, pp. 834–841.

[20] W. Lu, S. Hu, X. Liu, C. He, and Y. Gong, "Incentive Mechanism Based Cooperative Spectrum Sharing for OFDM Cognitive IoT Network," *IEEE Transactions on Network Science and Engineering*, vol. 7, no. 2, pp. 662–672, Apr. 2020.

[21] M. F. Khan and K. L. A. Yau, "Route Selection in 5G-based Flying Ad-hoc Networks using Reinforcement Learning," in *Proceedings of* 10^{th} *IEEE International Conference on Control System, Computing and Engineering (ICCSCE)*, Sep. 2020, pp. 23–28.

Pallav Kr. Deb He is a Ph.D. Research Scholar in the Department of Computer Science and Engineering, Indian Institute of Technology Kharagpur, India. He received his M.Tech degree in Information Technology from Tezpur University, India in 2017. Prior to that, he has completed the B. Tech degree in Computer Science from the Gauhati University, India in 2014. The current research interests of Mr. Deb include UAV swarms, THz Communications, Internet of Things, Cloud Computing, Fog Computing, and Wireless Body Area Networks. Further details are available in https://pallvdeb.github.io/

Anandarup Mukherjee He is currently a Senior Research Fellow and Ph.D. Scholar in Engineering at the Department of Computer Science and Engineering at Indian Institute of Technology, Kharagpur. He finished his M.Tech and B.Tech from West Bengal University of Technology in the years 2012 and 2010, respectively. His research interests include, but are not limited to, networked robots, unmanned aerial vehicle swarms, Internet of Things, Industry 4.0, 6G and THz Networks, and enabling deep learning for these platforms for controls and communications. His detailed profile can be accessed at http://www.anandarup.in

Sudip Misra (M'09–SM'11) He is a Professor with the Department of Computer Science and Engineering, Indian Institute of Technology, Kharagpur. He received his Ph.D. degree in Computer Science from Carleton University, in Ottawa, Canada, and the masters and bachelor's degrees, respectively, from the University of New Brunswick, Fredericton, Canada, and the Indian Institute of Technology, Kharagpur, India. Dr. Misra is the Associate Editor of the IEEE Transactions Mobile Computing and IEEE Systems Journal, IEEE Transactions on Sustainable Computing, IEEE Network, and Editor of the IEEE Transactions on Vehicular Computing. His current research interests include algorithm design for emerging communication networks and Internet of Things. Further details about him are available at http://cse.iitkgp.ac.in/ smisra/.